Title

Importance and challenges of environmental ligand binding and exchange: Introducing single molecule imaging as a model characterization technique

Authors

Saleh, Navid B
Das, Dipesh
Plazas-Tuttle, Jaime
et al.

Publication Date

2017-04-01

DOI

10.1016/j.impact.2017.03.005

Peer reviewed

NanoImpact 6 (2017) 90–98

Contents lists available at ScienceDirect

NanoImpact

journal homepage: www.journals.elsevier.com/nanoimpact

Frontier article

Importance and challenges of environmental ligand binding and exchange: Introducing single molecule imaging as a model characterization technique

Navid B. Saleh [a], Dipesh Das [a], Jaime Plazas-Tuttle [a], Darwin Yang [b], Jackson Travis Del Bonis-O'Donnell [b], Markita P. Landry [b,c,*]

[a] Department of Civil, Architectural and Environmental Engineering, University of Texas at Austin, Austin, TX 78712, United States
[b] Department of Chemical and Biomolecular Engineering, University of California-Berkeley, Berkeley, CA 94720, United States
[c] California Institute for Quantitative Biosciences (qb3), University of California-Berkeley, Berkeley, CA 94720, United States

ARTICLE INFO

Article history:
Received 17 January 2017
Received in revised form 22 March 2017
Accepted 24 March 2017
Available online 27 March 2017

ABSTRACT

Highly surface active nano-scale materials, when released into the natural environment, tend to adsorb geo- and bio-macromolecules and end up presenting a modified interface to biological species. Capped nanocrystals and polymer/surfactant modified nanomaterials also are known to undergo ligand exchange when exposed to natural systems. Thus, nano-bio interactions will primarily be governed by the adsorbed or exchanged natural macromolecules. To-date there has been no established technique determining the kinetics of ligand exchange or characterizing the bound geo-biomacromolecular corona in an environmental setting. Single-molecule imaging utilizing near-infra red spectrometry, and single-molecule imaging of fluorophore-tagged polymeric ligands can enable detailed characterization of biopolymeric corona. This perspective aims to highlight the importance of ligand exchange, identify roles of surface ligands on nano-bio interaction, and present initial evidence of macromolecular characterization on nanotube surfaces using single-molecule techniques. This commentary also aims to outline the challenges facing nano-environmental health and safety community on assessing biological interaction with complex nano-scale heterostructures in a realistic environmental matrix.

Published by Elsevier B.V.

1. Introduction

Physicochemical transformation of nanomaterials (NMs) is inevitable when released into the natural environment (Lowry et al. 2012), which strongly influences the interaction of these surface-active materials at the environmental and biological interfaces (Louie et al., 2016a). Geo- and bio-macromolecules present in natural waters will interact with NM surfaces and will adsorb either via direct binding onto pristine or covalently functionalized materials or by replacement of pre-existing engineered ligands of capped nanocrystals (Amal et al., 1992; Diegoli et al., 2008; Keller et al., 2010; Zhou and Keller, 2010; Zhang et al., 2009; Yang et al., 2009; Wang et al., 2010). Thus, biological systems and their membranes will interact with NMs first at the interface of the geo- or bio-molecular corona the NM has accrued prior to reaching the biological structure in question. Detailed characterization of this corona is essential for nano environmental health and safety (EHS) studies in complex but realistic natural environmental conditions.

Reduction in free energy by bringing in a monomer to a surface has been identified to be relatively large compared to its thermal energy, hence is known to drive macromolecular adsorption onto colloidal surfaces (De Gennes, 1987). Naturally occurring geo- and bio-macromolecules are subjected to solid-liquid distribution in geochemical systems due to their amphiphilicity. During adsorption process a net reduction in free energy is achieved by expulsion of water molecules; this is attained via a reduction in enthalpy (through elimination of van der Waals forces between water molecules and hydrophobic components), which is somewhat compromised by entropic loss (via dislodgement of oriented water molecules) (Lowry et al., 2012). Presence of high surface area NMs when suspended in natural waters (Tanford, 1980) enhances this adsorption process. NOM when at the vicinity of a surface introduces strong van der Waals interaction between the sorptive surface and the sorbing high molecular weight macromolecule (Schlautman and Morgan, 1994). Furthermore, hydrogen bonding between the NOM functional groups and surface moieties can drive macromolecules toward interfaces (Lau et al., 2013). Thus, preferential adsorption of NOM onto uncoated NM surfaces is a likely outcome, which will govern the interfacial interaction of these materials in the environment.

* Corresponding author at: Department of Chemical and Biomolecular Engineering, University of California-Berkeley, Berkeley, CA 94720, United States.
E-mail address: landry@berkeley.edu (M.P. Landry).

http://dx.doi.org/10.1016/j.impact.2017.03.005
2452-0748/Published by Elsevier B.V.

Metal and metal oxide nanocrystals are mostly capped with polymers and polymeric surfactants. The interaction of these pre-existing ligands with naturally occurring macromolecules may undergo via partial or complete ligand exchange (Lowry et al., 2012). Such exchange will be dictated by ligand and macromolecular types and will be modulated by the surrounding environmental matrix. Energetic gain due to replacement of relatively smaller ligands with larger NOM (Lau et al., 2013) or reaction (Murphy et al., 1990; Parfitt et al., 1977) of humic functional moieties with those at the capping agents will determine the kinetics and extent of ligand exchange. Furthermore, NM physicochemical properties will also influence NOM adsorption and ligand exchange processes (Aich et al., 2014), where complexity in emergent nano-heterostructures present an additional degree of complexity (Aich et al., 2014; Plazas-Tuttle et al., 2015; Saleh et al., 2015; Saleh et al., 2014). These key factors of the ligand exchange process will eventually result in the evolution of NM surface chemistry and thus the eventual nano-bio interaction.

Irrespective of whether the NOM will bind to NM surfaces by adsorption or via ligand exchange, the corona formed on these surfaces necessitate detailed characterization. To-date, indirect approaches have been utilized in characterizing geo- and bio-macromolecules on NM surfaces; e.g., Tracking protein, surfactant, and polymer coatings has been accomplished via attenuated total reflection-FTIR, absorption, and bulk fluorescence techniques, which have evaluated desorption of these ligands from various nanomaterial surfaces (Mudunkotuwa and Grassian, 2015; Jain et al., 2015; Louie et al., 2016b; Tsai et al., 2011; Smith et al., 2015). Additionally, calorimetry has been used in conjunction with electrophoresis to measure protein adsorption on NM, and small angle neutron scattering experiments to measure nanomaterial-adsorbed polymers (Cosgrove et al., 1987; Cárdenas et al., 2005). Fourier transformed infrared (FTIR) spectroscopy (Karajanagi et al., 2004), interfacial force measurements (Treuel and Nienhaus, 2012), ellipsometry (Byrne et al., 2008), contact stylus instruments (Consiglio et al., 1998), are prominent experimental techniques while theoretical modeling (Phenrat et al., 2008) of bound NOM layers provide further insight into these complex corona. However, a robust technique is yet to be developed to directly characterize the conformation of the macromolecules on NM surfaces, kinetics of ligand exchange, and extent of macromolecular adsorption or exchange. Although many tools exist to characterize both NMs and the interfacial synthetic or biological coronas (Sapsford et al., 2011), these methods are currently unable to give a detailed picture of biomolecular structure at the nano-bio interface (Nel et al., 2009). As a result, the molecular basis for local electronic properties, bioavailability, toxicological effects, structure and conformation of biomolecules on NMs remain unclear (Shvedova et al., 2010; Hauck et al., 2008).

Single-molecule imaging, utilizing near-infra red spectrometry and visible fluorophores, can enable detailed characterization of optically dense biopolymeric corona (Beyene et al., 2009). Single molecule imaging is a powerful technique to study individual molecules and singular intermolecular interactions (Zhang et al., 2013; Bisker et al., 2016). In particular, single-molecule fluorescence microscopy can be used to study individual polymers and macromolecules and their interactions both in vitro (Kruss et al., 2014; Wong et al., 2016) and in biologically complex environments (Giraldo et al., 2015; Giraldo et al., 2014; Landry et al., 2014). Single-molecule total internal reflection fluorescence microscopy (smTIRF) can achieve sub-diffraction limited imaging resolution by imaging molecules within a ~100 nm-deep field of view that is excited by an evanescent field, thereby eliminating signal from out-of-focus fluorophores. smTIRF allows nanometer spatial resolution and millisecond temporal resolution of single fluorescently-labeled polymers. As we show here, we can extend this technique to also spatially and temporally resolve interactions of polymers, and ligands, both among themselves and with synthetic nano-scale materials (Jain et al., 2011).

The focus of this perspective is to introduce single molecule imaging as an effective technique for bio-corona characterization. Differences in NOM chemical composition based on variation in natural water compartments is characterized, and the role of corona composition on environmental and nano-bio interaction is also analyzed. This article also highlights the challenges associated with characterization of complex nano heterostructures. A brief description of single molecule imaging with smTIRF and preliminary corona characterization data are presented. Strategies are discussed for adoption and utilization of this technique to study the detailed kinetics, extent and conformation of natural macromolecule adsorption, and corona formation on NM surfaces.

1.1. Environmental macromolecules and ligand exchange

The chemistry of naturally occurring bio- and geo-macromolecules widely vary depending on the phase of origin, i.e., terrestrial vs. freshwater or marine aquatic environment, and other environmental parameters (Niederer et al., 2007). These natural macromolecules can be broadly classified as non-humified (that originate from minor alteration via decay of tissue from living organisms) and humified (that are decomposition products of non-humified constituents) substances (Mulder et al., 1994). Carbohydrates, amino acids, proteins, lignin, hormones and low molecular organic acids are the first degradation products or non-humified substances that decomposes further to humified humic acids, fulvic acids, and humins (the combination is known as NOM). Among these natural macromolecules, NOM and polysaccharides are the most ubiquitous, which also are composed of a wide variety of functional groups and can demonstrate anionic/cationic as well as hydrophilic/hydrophobic behavior, depending on their chemical structure (Vannote et al., 1980; Mao et al., 2000). Thus, appreciation of the complex and variable chemistry of the geo- and bio-macromolecules when studying NM interaction is critical.

In a natural water body, the organic components can either be dissolved or suspended as particulates. The non-humic substances originate from viable cells and are relatively amenable to degradation, which generate altered molecular structure of new aquatic organic substances (Jose, 2009). Among these non-humified substances, carbohydrates are the most ubiquitous. These can be present as simple monosaccharide structures (composed of 3 to 6 carbon atoms) (Aich et al., 2014) or more complex branched polysaccharides (generally composed of 40 to 3000 carbon atoms) (Aich et al., 2014). Among these carbohydrates, monosaccharides and disaccharides are the water soluble and biodegradable fractions (Pigman, 2012); whereas, starch and glycogen, the primary energy sources of plants and animals, respectively, are the most biodegradable fractions in polysaccharides (Pigman, 2012). The availability of primary and secondary hydroxyl groups in starch and glycogen makes these polysaccharides hydrophilic in nature (Lu et al., 2009). Other polysaccharides such as cellulose and chitins, on the other hand, are not readily biodegradable and neither are water soluble. These carbohydrates are comprised of uniform glucose structures which allow these to resist enzymatic breakdown (O'Sullivan, 1997).

Proteins with amino acids as the primary building block (with amines and carboxyl functional moieties) are another important macromolecule in the aquatic environment, that can be structurally complex and can exhibit variation in surface charge (cationic, anionic, or nonionic) (Goldenberg and Steinberg, 2010). Amino acids, such as cysteine and other proteins containing cys-residuals also possess thiol functional groups (Trivedi et al., 2009), which enhance the affinity of these bio macro-molecules for some metal and metals oxides surface that are reactive to such disulfide and thiol groups (Aryal et al., 2006). Based on the environmental conditions, these thiol-containing proteins can form disulfide bonds, which might entirely change the interaction with NMs. Another prominent source of these non-humic substances is EPS, which can be excreted by both unicellular and multicellular organisms. The chemical composition of EPS varies depending on the organism from which these are produced (Wotton, 2004; Decho, 1990; Flemming and Wingender, 2010). EPS is typically responsible for conditioning environmental surfaces to allow formation of biofilms on

granular media and sediments. Proteins and polysaccharides are the key components of EPS. Polysaccharides found in EPS can be either linear or branched and are primarily comprised of organic moieties such as *O*-acetyl, *N*-acetyl, succinyl, piruvyl as well as inorganic components such as sulfates and phosphates (Wingender et al., 1999). Other functional moieties such as amino, CH_2, and CH_3 groups are also be present in EPS (Wingender et al., 1999; Chen et al., 2013). The complexity in structure and variation in functional moieties of non-humified carbohydrates and proteins calls for attention when assessing nano-EHS.

Humic substances on the other hand, are heavily decomposed and cannot be biodegraded by most aquatic organisms. While humic and fulvic acids are mostly water soluble, humins are insoluble in water at environmental pHs (Thurman and Malcolm, 1981; Schnitzer, 1982). Humic substances can also demonstrate different elemental composition and physicochemical behavior depending on the aquatic environmental compartment of residence; i.e., ground water vs. surface water. Due to the presence of mineral collector surfaces in the subsurface, composition of NOM shows functional differences between the collector surfaces and porewater. Hydrophobic components of the NOM tend to adsorb onto mineral surfaces, leaving behind more hydrophilic components in the pore water as dissolved organic matter (Parfitt et al., 1977). In comparison, surface water tends to possess a higher quantity of unbound and mobile humic fraction with a larger presence of hydrophobic chemical moieties compared to groundwater. The origin of these macromolecules is also largely different between these compartments due to the differences in the presence of biota and microorganisms. For instance, the fulvic acids in groundwater have relatively lower oxygen content that those in surface water. The fulvic acids in the subsurface are also less aromatic in nature than those above surface because of a group of benzoate-metabolizing bacteria that resides in underground (Pettersson et al., 1994). Such physicochemical and structural difference in organics and macromolecules will thus play a significant role in modifying NM interaction with environmental interfaces (Murphy and Zachara, 1995).

1.2. NM interaction with macromolecules: knowledge gap and challenges

NMs can be released into the environment during their manufacturing process (Bello et al., 2008; Yeganeh et al., 2008), usage, and/or at the end-of-life disposal (Farkas et al., 2011; Geranio et al., 2009; Kaegi et al., 2010; Kaegi et al., 2008; Benn and Westerhoff, 2008; Benn et al., 2010; Hsu and Chein, 2007; Köhler et al., 2008), as well as can pass through wastewater facilities (Kiser et al., 2009; Kaegi et al., 2011). The EHS of these NMs thus is strongly affected by the environment these are released into or eventually might end up in. While studying the NM-macromolecule interaction, the general focus is on overall environmental conditions, i.e., typical composition of water in surface water or groundwater. These conditions can be considered relatively mild compared to extreme environments such as landfills, estuaries, and marshes. Non-humic and humic composition can vary widely in these environments, modulated by different organisms that reside in the respective areas. For example, landfills are repositories of abandoned products over a long period of time thus house a high concentration of organics compared to natural water and most soils (Kulikowska and Klimiuk, 2008). Marshes have stagnant water also with high concentration of organic matter (Tanner et al., 1998). Estuaries and coastal regions are highly saline and are perfectly conditioned for destabilizing colloidal particles and engineered NMs. It is extremely challenging to mimic such extreme conditions in the lab scale while studying the NM-macromolecule interaction. Hence, researchers have tried addressing such interaction with rather simple experimental designs. Several studies have highlighted the importance of NOM and complexity in NOM chemistry on aggregation, transport, and toxicological behavior of NMs (Afrooz et al., 2013a; Afrooz et al., 2013b; Aich et al., 2016; Khan et al., 2013; Khan et al., 2015a; Saleh et al., 2008; Afrooz et al., 2016; Lin et al., 2010; Kang et al., 2009; Baalousha et al., 2008; Hotze et al., 2010). However, most of these studies use standardized humic and fulvic acids (e.g., Suwanee River humic acid and NOM) as representative NOMs nano-EHS studies (Afrooz et al., 2013a; Afrooz et al., 2013b; Aich et al., 2016; Khan et al., 2013; Khan et al., 2015a; Saleh et al., 2008; Afrooz et al., 2016) and analyze the role NOM adsorption on nano-EHS. Though the complexity in NOM chemistry is appreciated in literature, little attention has been given to deconvolute the real-life complexity of NOMs.

Complexity of NM interaction in natural environment further increases from the presence of pre-existing surface coatings on engineered NMs, which are intentionally introduced to particle surfaces for achieving higher colloidal stability (Buffle et al., 1998). Small charged molecules (e.g., citrate) and larger synthetic macromolecules, polymeric surfactants, polyelectrolytes (e.g., poly acrylic acid), or non-ionic polymers (e.g., polyvinylpyrrolidone) are the most commonly used capping agents for engineered NMs(Rao et al., 2006). Surfactants and polymers can be anionic, cationic, zwitterionic, and nonionic (Somasundaran and Krishnakumar, 1997), and can either be chemically bound via covalent bonding (Zeng et al., 2006; Chao et al., 2006), physisorbed by electrostatic or short ranged hydrophobic interactions (Khan et al., 2015b; Aich et al., 2013), or grafted (Kumar et al., 2013) onto or from the NM surfaces. Different biomolecules are also introduced on NM surfaces as stabilizers, primarily in biomedical and therapeutic applications (Wang et al., 2009); such biomolecules include: nucleic acids (i.e., DNA/RNA/PNA/LNA as genes, oligomers, aptamers, ribozymes/DNAzymes), antibody, fatty acids, lipids, mono and polysaccharides, different types of proteins, and peptides (Sapsford et al., 2013).

The data gap in this literature further exacerbates via the expansion in the material space and development of complex nano-heterostructures (Rigdon and Huang, 2014; Das et al., 2016). These heterostructures can be classified as carbon-carbon, carbon-metal, core-shell meta-metal, among others (Aich et al., 2014). Conjugation of multiple NMs result in the emergence of unique and synergistic electrical, optical, mechanical, catalytic, sensing ability and magnetic properties, and are being used for a wide range of applications in biomedical and nanotherapeutics, electro- and photo-catalysis (Eder and Windle, 2008), electronics (Alley et al., 2012), gas sensing (Llobet et al., 2008), biosensing (Liu et al., 2008), laser technology (Zhu et al., 2006) and other emerging areas. Upon hybridization, these novel heterostructures have demonstrated emergent properties, which are different more than the sum of parts; e.g., hybridization of TiO_2 with carbon nanotubes lowers band gap of the heterostructures and thus exhibits enhanced photocatalytic activity (visible photo-activation) and ROS generation compared to component TiO_2 and CNTs (Jung et al., 2002). The intrinsic van der Waals interaction energy of NMs are also found to be altered via hybridization (Hua et al., 2016) and will likely result in unknown interaction of the NHs with environmental interfaces (i.e., aggregation, deposition, and toxicity).

In order to address such wide data gap and reduce uncertainties in EHS studies, the field has utilized a wide range of state-of-the-art analytical techniques to characterize NM surfaces. In this quest, shift in NM surface Plasmon resonance due to the NOM, protein, and biopolymer binding has been monitored (Diegoli et al., 2008; Lundqvist et al., 2004). Ellipsometry (Brewer et al., 2005), total reflection infrared spectroscopy (Yang et al., 2005; Vargas et al., 2011), atomic force microscopy (Kim et al., 2003) combined with flow field fractionation (Baalousha and Lead, 2007a; Baalousha and Lead, 2007b), contact stylus instrument (Consiglio et al., 1998), nuclear magnetic resonance with size-exclusion chromatography (Hellstrand et al., 2009), and other optical techniques such as dynamic light scattering (Inomoto et al., 2009), circular dichroism (You et al., 2005) have been applied to analyze adsorbed macromolecular layer thickness, ligand conformation, etc. Many of these techniques have effectively captured the protein/polymer layer thickness on the NM surfaces, however, have yet to successfully characterize ligand exchange and corona structure on NM surfaces. Ligand exchange is a dynamic process and depends on the thermodynamics of the system; thus, rate and extent of exchange need to be quantified. Moreover,

NM-macromolecular corona conformation is also dynamic and is dependent on the chemistry of the macromolecule being exchanged as well as the surface chemistry of the NMs. A robust analytical technique is thus necessitated that can characterize time-dependent macromolecular exchange as well as conformation of the corona to complete our understanding at the nano-bio interface.

1.3. Probing the bio-accessibility of nanoparticle-ligand conjugates

1.3.1. Single-molecule visualization of polymeric ligands on nanomaterial surfaces

We introduce a smTIRF-based microscopy platform (Roy et al., 2008) to probe transient interactions of bio-macromolecules on a NM surface at the single-molecule level. In this platform, fluorophore-labeled polymeric ligands serve to quantify and track in real-time the binding strength, binding kinetics, and propensity for ligand exchange of NM-adsorbing polymers on the surface of a single-walled carbon nanotube (SWNT) with unprecedented precision. We show that individual nanotube-bound polymeric ligands can be tracked in their interactions with a competing unlabeled ligand, resulting in partial desorption of the original ligand from the nanotube. Fluorescence microscopy is used to track the degree to which a competing ligand induces desorption of the original ligand, thus enabling a quantitative assessment of ligand binding to—and displacement of—a polymer-encapsulated nanoparticle. In our example, we use the known hybridization affinities of one DNA sequence with its complementary sequence to test the ability of smTIRF and visualize the hybridization process. In this manner, nanotube-bound polymeric ligands are imaged via with smTIRF to observe the position and distribution of polymer ligands on the NM surface. In this platform, fluorescent polymeric ligands are adsorbed onto a SWNT surface, and the resulting polymer-SWNT moiety is surface-immobilized on a functionalized microscopy flow chamber. The polymer-SWNTs can then be studied in real-time upon exposure to different environmental conditions, controlled by fluid exchange in the ~200 μL microscopic imaging channel (Harvey et al., 2017).

Here, we present the visualization of three distinct polymer ligands adsorbed to the surface of SWNT: (i) Fifteen single-stranded DNA polynucleotide repeats of GT followed by a thirty-base random sequence ($(GT)_{15}$-Rnd_{30}), (ii) fifteen consecutive GT repeats followed by a sixteen-base random sequence labeled with Cyanine 5 ($(GT)_{15}$-Rnd_{16}-Cy5), and (iii) Rhodamine B isothiocyanate (RITC) labeled polyethylene glycol (RITC-PEG-RITC). $(GT)_{15}$ was chosen as a base sequence because each of the 30 aromatic bases of the $(GT)_{15}$ polymer provides a series of pi-stacking anchors for adsorption to the SWNTs, as we've shown previously (Landry et al., 2015). Conversely, the RITC-PEG-RITC block copolymer only has two aromatic ends which can pi-stack to the SWNT, flanking a hydrophillic 5000 Da polyethylene glycol chain that does not interact with SWNT surface. Thus, the effects of a strongly-NM adsorbing $(GT)_{15}$ and a weakly-NM adsorbing RITC-PEG-RITC polymer can be independently studied. The Cy3 fluorophore, and RITC fluorophores, will quench when adsorbed to the SWNT due to fluorescence resonance energy transfer, and are expected to de-quench if desorbed from the SWNT.

Polymer-adsorbed nanotubes were prepared via non-covalent adsorption of the polymeric ligand onto the nanotubes as described in Materials and methods. Briefly, 0.2 mg $(GT)_{15}$-Rnd_{30} or $(GT)_{15}$-Cy3 DNA polymers were mixed in a w/w 2:1 ratio with HiPCO SWNT in 1 mL 100 mM NaCl. The mixture was ultra-sonicated via tip sonication and subsequently purified via centrifugation to recover individually-dispersed $(GT)_{15}$-Cy3 DNA-SWNT complexes (see Supplemental Fig. S2). The RITC-PEG-RITC polymer was adsorbed onto SWNTs, first by sonicating 0.2 mg of HiPCO SWNT with a w/w excess of sodium dodecyl sulfate (SDS) and subsequently exchanging the SDS corona for RITC-PEG-RITC at a concentration of 60 mg/mL with a 10 kDa dialysis membrane in PBS buffer. Subsequent purification yielded individually-dispersed RITC-PEG-RITC-SWNT. Microfluidic imaging chambers for smTIRF microscopy were prepared using a BSA-biotin and NeutrAvidin surface immobilization protocol, as described previously (Chio et al., 2017; Landry et al., 2017).

1.3.2. Imaging and quantifying DNA duplex formation on single SWNT

Non-fluorescent surface-immobilized $(GT)_{15}$-Rnd_{30}-SWNT were imaged via the addition of a short fluorescently-labeled single-stranded DNA oligonucleotide complementary to the 30-base random sequence carrying a 3′-terminally labeled Cy5 fluorophore tag Cy5-$cRnd_{30}$. The appearance of fluorescence on the imaging surface thus corresponds to instances of DNA hybridization in which partial desorption of the Rnd_{30} polymer from the SWNT results from DNA hybridization by a complement strand. The test system of DNA strands, one originally bound to a SWNT, interacting via hybridization serves as a proxy for using smTIRF to study ligand-nanoparticle interactions. Fig. 2 shows the imaging surface upon addition of Cy5-$cRnd_{30}$ to surface-immobilized $(GT)_{15}$-Rnd_{30}-SWNT. Our imaging platform resolves Cy5-duplex labeled nanotubes, whereby the fluorescent signal originates from the in-situ hybridization of Cy5-cDNA to the random 30 base ssDNA sequence on the SWNT ($(GT)_{15}$-Rnd_{30}-SWNT). We highlight that Cy5 cDNA hybridization results in a partial desorption of the ssDNA strand wrapping the SWNT with a hybridized duplex attached, and does not constitute a full desorption of the DNA from the SWNT. In Fig. 2, the duplexes formed resulted in 103 fluorescent nanotubes within the sample field, in contrast to no fluorescence emission from the $(GT)_{15}$-Rnd_{30}-SWNT only or Cy5-$cRnd_{30}$ only samples. We thus conclude that the association between the Cy5-labeled Cy5-cDNA oligonucleotide and the nanotube is due to DNA hybridization only, without non-specific adsorption of the oligonucleotide. The photobleaching of Cy5 fluorophores can be used to determine the number of unique duplexes per diffraction-limited DNA-SWNT spot. The intensity-time trace of a particular single nanotube shows discrete steps of comparable intensity corresponding to the photobleaching of 4 Cy5 molecules on the nanotube surface (Fig. 2d). Because each duplex contains a single fluorophore, the number of photobleaching steps observed per molecule represents the number of duplexes formed per functionalized nanotube. The number of duplexes per DNA-SWNT follows a non-normal skewed distribution with most SWNT spots showing 2 hybridized duplexes per SWNT, and anywhere between 1 and 4 duplexes observed per SWNT (Fig. 2e, f). Adsorbing a low density of SWNT on the imaging surface ensures that most SWNT emitters within a ~300 nm diffraction-limited spot will exist as singular SWNT per spot. However, we highlight that a small proportion of fluorescent spots could result from multiple SWNT within a diffraction-limited spot. As such, our platform enables direct optical tracking of ligands on nanomaterials. This imaging technique can thus be leveraged to study the adsorption of one ligand to another, demonstrated here by the hybridization of one DNA oligonucleotide to its SWNT surface-adsorbed complement (Fig. 1).

1.4. Quenching & de-quenching of pi-stacked dyes as proxy for polymer conformation on SWNT surface

1.4.1. Imaging polymer desorption from a single SWNT via DNA hybridization

Quenching of organic fluorophores such as Cyanine 5 (Cy5), or RITC occurs as a function of proximity to the surface of SWNTs (Yang et al., 2008), thereby creating a fluorescent ruler to quantify the degree of polymer desorption at a single-molecule scale. Quenching of fluorophores is expected for fluorophores adsorbed to the SWNT surface via pi-stacking, whereas brightening of fluorophores is expected from fluorophore de-quenching if the associated polymeric ligand partially desorbs from the surface. Surface-immobilized $(GT)_{15}$-Rnd_{16}-Cy5-SWNT were imaged prior to (Fig. 3a) and after (Fig. 3b) the addition of unlabeled $cRnd_{16}$ oligonucleotide. $(GT)_{15}$-Rnd_{16}-Cy5-SWNT initially exhibit a large degree of Cy5 fluorophore quenching due to Cy5 pi-stacking to the SWNT surface. Addition of $cRnd_{16}$-oligonucleotide

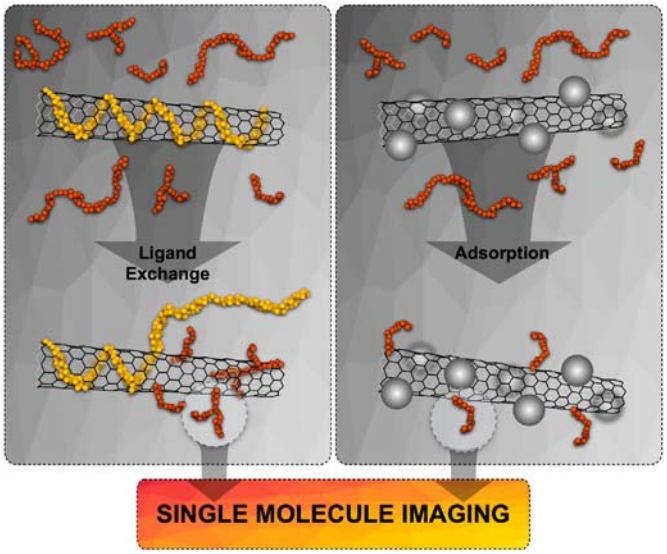

Fig. 1. Schematic representing macromolecular adsorption and ligand exchange on NM surfaces, which can be systematically characterized with single molecule imaging.

promotes de-stacking of the Cy5 fluorophore via hybridization of the fluorophore-labeled $(GT)_{15}$-Rnd_{16}-Cy5-SWNT, and results in de-quenching of the terminal Cy5. An average of N = 50 image captures shows the addition of $cRnd_{16}$ increases the number of de-quenched Cy5 by 69.3%, from 242 ± 67 Cy5 spots, to 410 ± 68 Cy5 spots (Fig. 3c, error is standard error). As such, our platform allows quantification of the displacement of a polymeric ligand, $(GT)_{15}$-Rnd_{16}, by a competing sequence-specific ligand, $cRnd_{16}$, on the surface of a single-walled carbon nanotube.

1.4.2. Imaging polymer desorption from a single SWNT via ligand disruption

Here, we imaged surface-immobilized RITC-PEG-RITC SWNT and tested the change in the RITC-PEG-RITC ligand adsorption upon exposure to a competing ligand, estradiol. A 5 mg/L solution of RITC-PEG-RITC SWNT were surface-immobilized in a microfluidic chamber with the same surface-adsorption scheme used for DNA-SWNTs (see Materials and methods) within a ~200 μL volume, and initial RITC diffraction-limited fluorescent spots were counted. To quantify the conformation of the RITC-PEG-RITC polymer with respect to its SWNT surface-adsorption, we counted the number of diffraction-limited SWNT molecules and RITC molecules in the absence or presence of 500 μM estradiol. Upon addition of 500 μM estradiol, we observe a 12% increase in the number of fluorescent RITC molecules per imaging field of view, from 271.7 ± 4.5 to 304.5 ± 4.4; mean ± SE (Fig. 4). We hypothesize that RITC fluorescence increase upon estradiol exposure is a result of the intercalation of estradiol between the aromatic carbons of the SWNT surface, and the RITC fluorophores of the RITC-PEG-RITC polymer. The physical intercalation of the estradiol analyte may yield separation between the SWNT surface and the RITC-PEG-RITC polymer without causing polymer desorption, thereby causing RITC de-quenching. A similar perturbation without full DNA polymer desorption was observed for DNA hybridization on SWNT in Figs. 2 and 3. This direct relationship between a nanoparticle's polymeric corona fluorescence and interaction with a competing (unlabeled) ligand may enable quantification of NOM adsorption to a polymer-functionalized nanoparticle. While this platform is presented as a modular interaction and partial displacement of a singular polymeric structure on a SWNT surface by a ligand, it can readily be extended to quantify multiple ligand-NOM interactions. Furthermore, smTIRF enables direct visualization and quantification of partially-desorbed phases, which is a missing dimension in the bulk corona ligand exchange described below. As such, we can use smTIRF microscopy to quantify the degree of polymer ligand disruption from its nanomaterial-adsorbed phase, when exposed to a competing ligand. Together, smTIRF with existing bulk-phase techniques can provide a full picture of partially and fully desorbed nanoparticle corona phases, and the extent to which these phases are perturbed by NOM ligands.

1.4.3. Bulk characterization of nanoparticle corona ligand exchange: UV–Vis-IR spectroscopy

Orthogonal to smTIRF visualization of polymeric ligand corona exchange, UV–Visible-Near Infrared absorption spectrometry, and near-infrared fluorescence emission spectrometry, can be utilized to validate the occurrence and degree to which a nanoparticle corona is exchanged for another ligand in bulk. Here, we compare the adsorption of either a

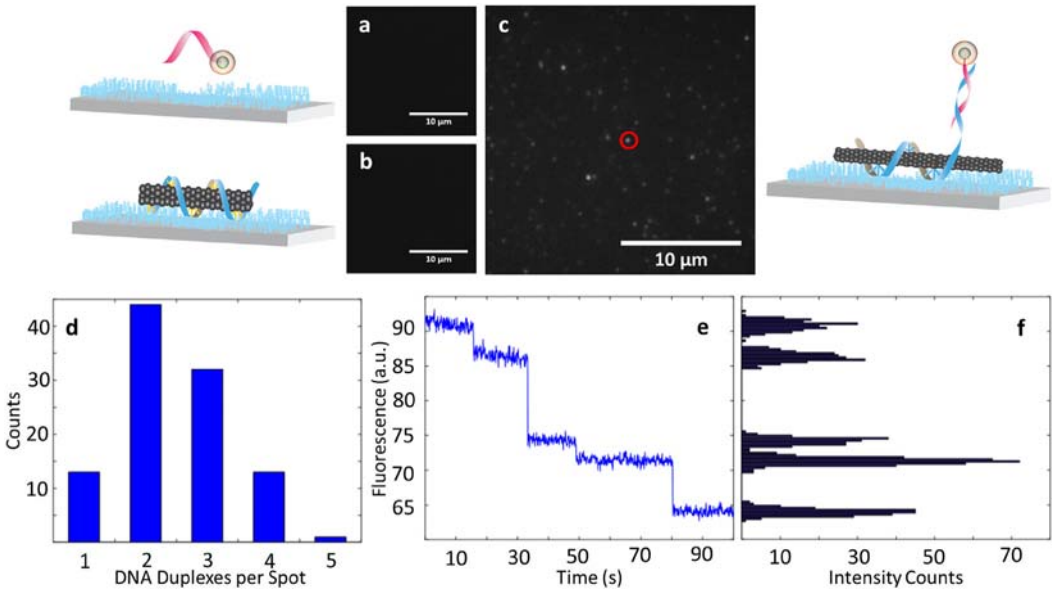

Fig. 2. (a) Cy5-$cRnd_{30}$ only and (b) $(GT)_{15}$-Rnd_{30}-SWNT only, on the imaging surface, show no fluorescence (c) Fluorescence is due to Cy5 specifically, not due to non-specific adsorption of contaminants or stray Cy5-$cRnd_{30}$ (n > 20 for all controls) (d) counts per SWNT spot of Cy5 intensity quenching enable quantification of DNA duplexes formed per SWNT spot. Corresponding (e) Intensity time trace (100 ms time resolution) of a Cy5-cDNA hybridized to an immobilized $(GT)_{15}$-Rnd_{30}-SWNT complex shows 4 photobleaching steps and corresponding (f) fluorescence intensity counts, each representing to a unique Cy5-cDNA ligand.

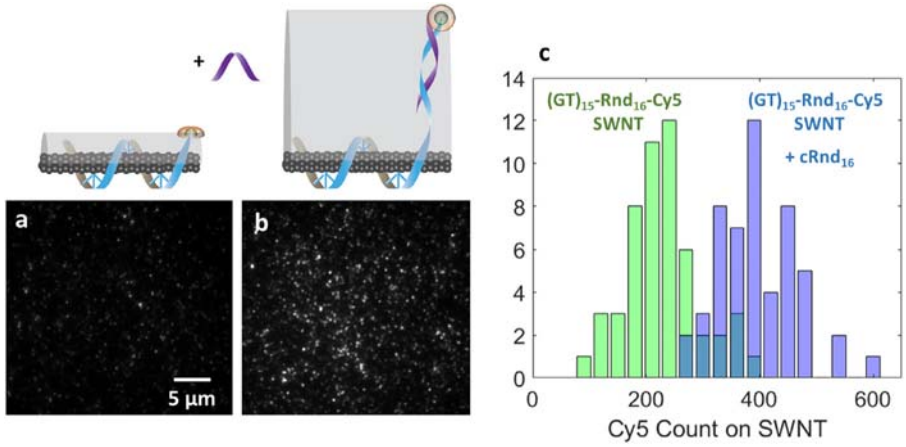

Fig. 3. smTIRF fluorescence microscopy of DNA-carbon nanotubes. (a) Nanotubes encapsulated with $(GT)_{15}$-Rnd_{16}-Cy5 polymer ligand show quenched Cy5 fluorescence (b) addition of $cRND_{16}$ hybridizes to the $(GT)_{15}$-Rnd_{16}-Cy5 and results in Cy5 de-stacking from the SWNT, and de-quenching in the fluorescence microscope (scale bar 5 μm). (c) Quantification of all fluorescent ligands on all nanotubes in the sample shows an increase in de-quenched fluorescent SWNT spots after addition of unlabeled $cRnd_{16}$.

RITC-PEG-RITC polymeric ligand, or sodium cholate (SC) surfactant, to SWNT. Using our RITC-PEG-RITC ligand adsorption to SWNT as a proxy, we demonstrate quantifiable tracking of RITC-PEG-RITC ligand exchange with a sodium cholate SWNT corona. Briefly, we first create a suspension of SC-adsorbed SWNT in water, using a 0.2 mg mass of HiPCO SWNT and a w/w excess, 2% solution of SC probe-tip sonicated for 1 h at 10 W power. Excess RITC-PEG-RITC is removed from solution through centrifugal filtration with a 100 kDa molecular weight cutoff prior to experimentation. The absorption (Fig. 5a) and fluorescence emission (Fig. 5b) spectra of 80 mg/L RITC-PEG-RITC-SWNT show distinct peaks, each corresponding to a unique electronic transition within the SWNT, whose magnitude and frequency can be modulated by the dielectric SWNT environment. We show that the difference between a SC SWNT-adsorbed phase, and a RITC-PEG-RITC SWNT-adsorbed phase, can be quantified by a solvatochromic shift in peak values. Normalized absorbance spectra of SWNTs in the near-infrared region before and after corona phase exchange show that SWNT peaks corresponding to E_{11} transitions (multiple chiralities between 900 nm and 1300 nm) shift after replacement of SC by RITC-PEG-RITC on the SWNT surface, while E_{22} transitions (multiple chiralities between 600 and 900 nm) remain comparable. Correspondingly, the near-infrared fluorescence of the two samples also reflect a change in relative peak intensities, as well as a red-shift in RITC-PEG-RITC-SWNT peak wavelength, corresponding to a more polarizable environment provided by the PEG as compared to SDS.

2. Materials and methods

2.1. Materials

Raw HipCO (High-pressure Carbon Monoxide synthesis process) SWNTs were purchased from NanoIntegris (batch #HR27-104). All cyanine dye (Cy3 and Cy5) tagged ssDNA sequences were obtained from Integrated DNA Technologies (sequences below). Reagents were purchased from Sigma Aldrich unless otherwise specified. The following are polynucleotide sequences were used to encapsulate SWNTs, or to hybridize to DNA-encapsulated SWNTs, as noted below:

1) DNA = $(GT)_{15}$-Rnd_{30}, used to encapsulate SWNT:

5′ GTGTGTGTGTGTGTGTGTGTGTGTGTGT CTA AGG ATG CGT GTA TTG GTA GGA TCA GTT 3′

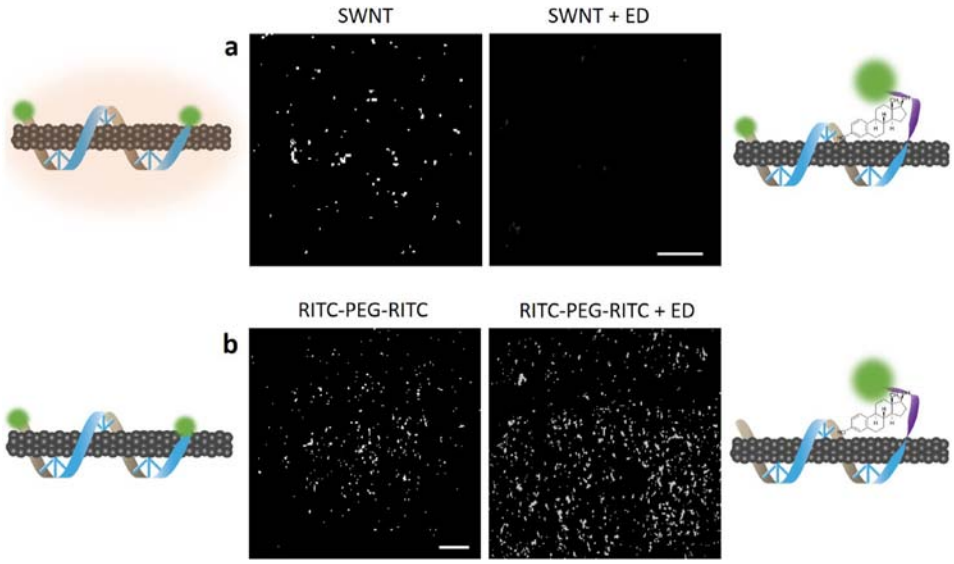

Fig. 4. Effect of estradiol on RITC-PEG-RITC: infrared SWNT fluorescence and visible RITC fluorescence. Upon addition of 500 μM estradiol to individually surface-immobilized RITC-PEG-RITC-SWNT (a) Near-infrared fluorescence of SWNT quenches with after exposure to estradiol. (b) Visible fluorescence of the RITC fluorophore de-quenches after exposure to estradiol. Scale 1 μm.

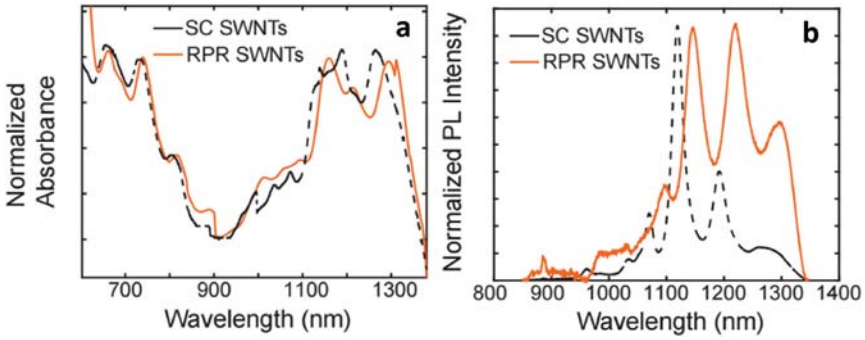

Fig. 5. UV–Vis-IR Absorption, and near-IR fluorescence spectroscopy characterization of RITC-PEG-RITC polymer ligands. (a) Absorption spectra of SWNT are red-shifted when RITC-PEG-RITC is adsorbed on the SWNT (orange), in comparison to sodium cholate adsorbed to SWNT (black, dashed). (b) Corresponding fluorescence emission spectra with 721 nm excitation of RITC-PEG-RITC adsorbed SWNT (orange) red-shifted in comparison to sodium cholate adsorbed to SWNT (black). Time between spectra is 1 h.

2) cDNA = Rnd_{30}-Cy5, hybridizes to DNA1 on SWNT:

5′ AAC TGA TCC TAC CAA TAC ACG CAT CCT TAG/Cy5/3′

3) DNA = $(GT)_{15}$-Rnd_{16}-Cy5-SWNT, used to encapsulate SWNT:

5′ GTG TGT GTG TGT GTG TGT GTG TGT GTG TGT CTA AGG ATG CGT GTA T/Cy5/3′

4) cDNA = $cRnd_{16}$, hybridizes to DNA1 on SWNT:

5′ ATA CAC GCA TCC TTA G 3′

2.2. DNA SWNT suspension

Solid SWNTs were added to a 100 mM NaCl solution in a 2:1 mass ratio with DNA. An Eppendorf tube containing 1 mL total volume of this mixture was placed in a cooling block and sonicated using an ultrasonic processor (Cole Parmer) with a 3 mm probe tip for 10 min at a power output of 6 W. The resulting suspension was incubated at room temperature for 30 min then centrifuged at 16,000 × *g*. 90% of the supernatant was collected so as to keep the pellet of SWNT aggregates intact. UV–Vis absorbance (GE Nanovalue Plus, Fairfield, CT) was used to determine the concentration in mg/L of SWNT suspensions.

2.3. smTIRF microscopy of immobilized SWNT suspensions

DNA SWNT suspensions were immobilized on the surface of a glass coverslip for fluorescence imaging. The surfaces of a glass microscope slide and #1.5 glass coverslip were washed using isopropanol and water and then were dried. Strips of double-sided tape were laid across the microscope slide in parallel rows, 0.5 cm apart. The coverslip was then placed on top creating distinct microfluidic channels with volumes of approximately 20 μL (see Fig. S1). Each channel was first washed with 100 μL of 100 mM NaCl solution by pipetting from one of the two openings and holding a Kimwipe on the other end to induce flow. Next, 50 μL of biotinylated bovine serum Albumin in 100 mM NaCl (Thermo Scientific, 1 mg/mL) was flowed through the channel. The BSA-biotin solution filled channel was incubated at room temperature for 5 min and then washed with 50 μL NaCl solution. The incubation and wash steps were repeated with NeutrAvidin (0.2 mg/mL, Thermo Scientific). Following rinsing of unbound NeutrAvidin, a 5 mg/L concentration of DNA-wrapped SWNTs were introduced into the imaging chamber, resulting in NeutrAvidin linked binding between DNA-SWNTs and the surface adsorbed BSA-biotin-NeutrAvidin, as described previously (Chio et al., 2017; Landry et al., 2017). Immediately before imaging, all channels were flushed with 50 μL of an oxygen scavenging buffer consisting of: 20 mM Tris (pH 8), 200 mM NaCl, 2 mM trolox, 0.16 mg/mL glucose oxidase, and 0.02 mg/mL catalase.

Microfluidic slides were imaged on a Zeiss Elyra microscope with a 100× TIRF objective. Cy3 and Cy5 were excited with laser of 561 nm and 642 nm wavelengths, respectively. A series of 1000 images were collected with 100 ms exposure. For samples which required imaging before and after hybridization, the complementary DNA was added in excess following the initial data collection. The channels were left to rest for 5 min and then washed with imaging buffer a second time. The channels were then immediately imaged again using the same laser and detector settings.

3. Conclusion

Current experimental tools fall short to probe the structure of polymeric ligands on the surface of NMs during the dynamic changes in aqueous environments. Our work outlines the development of a fluorescence microscopy-based platform, which allows spatial and temporal resolution of polymeric structure and activity at this interface. Carbon nanotube-encapsulated nucleic acids and synthetic PEG-based block co-polymers, designed to explore polymer-dependent affinity to the nano-surface, are observed via total internal reflection (TIR) microscopy at the single-molecule level. Taking advantage of the single fluorophore resolution that allows us to observe individual ligand interactions with a SWNT, our measurements reveal novel dynamic properties and inter-molecular interactions of nano-scale systems that are not measurable from ensemble experiments. The application of single molecule fluorescence microscopy to NM provides evidence that ligand susceptibility to (i) targeted interaction with another ligand, (ii) intercalation or perturbation by another ligand, or (iii) full exchange by a competing ligand, is a process that can be imaged and quantified in real-time with smTIRF and infrared spectrometry. This platform, validated by several example applications, is generally applicable for nano-bio systems to answer questions of ligand structure, adsorption affinity, exchange propensity, and could enable future studies in environmental remediation and toxicity. This is another powerful toolset that will aid in resolving geo- and bio-macromolecular complexity at NM-water interfaces. Appreciating the complexity of chemical functionality and heterogeneity of natural organic matter, we note here that successful utilization of this technique for NOM binding will largely depend on deciphering specific spectral signature upon binding. Furthermore, single-molecule techniques are optimally suited to study single or few interactions. As such, single-molecule imaging will be most useful in its application to study the interaction of NOM and NOM surrogates with nanoparticles. We propose that analysis of NOM with the novel single-molecule imaging technique ought to begin by utilizing NOM surrogate molecules (i.e., pyromellitic acid, salicylic acid, phthalic acid, thiol, and monosaccharide). Once relative nanomaterial-NOM surrogate binding

or displacement strengths have been characterized, the platform can be extended to analyze complex geo- and bio-macromolecular corona characterization.

Acknowledgements

This work was supported by a Burroughs Wellcome Fund Career Award at the Scientific Interface (CASI), the Simons Foundation, a BBRF young investigator award, and a Beckman Foundation Young Investigator Award (M.P.L.). It was also partially supported by National Science Foundation grant #1440261 (N.B.S.). D. Y. acknowledges support from an NSF GRFP fellowship. Research reported in this publication was supported in part by the National Institutes of Health S10 program under award number 1S10OD018136-01. The content is solely the responsibility of the authors and does not necessarily represent the official views of the National Institutes of Health.

Appendix A. Supplementary data

Supplementary data to this article can be found online at http://dx.doi.org/10.1016/j.impact.2017.03.005.

References

Afrooz, A.R.M.N., Khan, I.A., Hussain, S.M., Saleh, N.B., 2013a. Environ. Sci. Technol. 47, 1853–1860.
Afrooz, A.R.M.N., Sivalapalan, S.T., Murphy, C.J., Hussain, S.M., Schlager, J.J., Saleh, N.B., 2013b. Chemosphere 91, 93–98.
Afrooz, A.R.M.N., Das, D., Murphy, C.J., Vikesland, P., Saleh, N.B., 2016. Water Res. 99, 7–15.
Aich, N., Boateng, L.K., Flora, J.R., Saleh, N.B., 2013. Nanotechnology 24, 395602.
Aich, N., Plazas-Tuttle, J., Lead, J.R., Saleh, N.B., 2014. Environ. Chem. 11, 609–623.
Aich, N., Boateng, L.K., Sabaraya, I.V., Das, D., Flora, J.R., Saleh, N.B., 2016. 3562-3571. Environ. Sci. Technol. 50.
Alley, N.J., Liao, K.S., Andreoli, E., Dias, S., Dillon, E.P., Orbaek, A.W., Barron, A.R., Byrne, H.J., Curran, S.A., 2012. Synth. Met. 162, 95–101.
Amal, R., Raper, J.A., Waite, T., 1992. J. Colloid Interface Sci. 151, 244–257.
Aryal, S., Remant, B., Dharmaraj, N., Bhattarai, N., Kim, C.H., Kim, H.Y., 2006. Spectrochim. Acta A Mol. Biomol. Spectrosc. 63, 160–163.
Baalousha, M., Lead, J.R., 2007a. Environ. Sci. Technol. 41, 1111–1117.
Baalousha, M., Lead, J.R., 2007b. Sci. Total Environ. 386, 93–102.
Baalousha, M., Manciulea, A., Cumberland, S., Kendall, K., Lead, J.R., 2008. Environ. Toxicol. Chem. 27, 1875–1882.
Bello, D., Hart, A.J., Ahn, K., Hallock, M., Yamamoto, N., Garcia, E.J., Ellenbecker, M.J., Wardle, B.L., 2008. Carbon 46, 974–977.
Benn, T.M., Westerhoff, P., 2008. Environ. Sci. Technol. 42, 4133–4139.
Benn, T., Cavanagh, B., Hristovski, K., Posner, J.D., Westerhoff, P., 2010. J. Environ. Qual. 39, 1875–1882.
Beyene, A.G., Demirer, G.S., Landry, M.P., 2009. Current Protocols in Chemical Biology. John Wiley & Sons, Inc. http://dx.doi.org/10.1002/cpch.10.
Bisker, G., Dong, J., Park, H.D., Iverson, N.M., Ahn, J., Nelson, J.T., Landry, M.P., Kruss, S., Strano, M.S., 2016. Nat. Commun. 7, 10241.
Brewer, S.H., Glomm, W.R., Johnson, M.C., Knag, M.K., Franzen, S., 2005. Langmuir 21, 9303–9307.
Buffle, J., Wilkinson, K.J., Stoll, S., Filella, M., Zhang, J., 1998. Environ. Sci. Technol. 32, 2887–2899.
Byrne, T., Lohstreter, L., Filiaggi, M., Bai, Z., Dahn, J., 2008. Surf. Sci. 602, 2927–2935.
Cárdenas, M., Dreiss, C.A., Nylander, T., Chan, C.P., Cosgrove, T., Lindman, B., 2005. Langmuir 21, 3578–3583.
Chao, G., Wenwen, L., Yi Zheng, J., Hao, K., 2006. Nanotechnology 17, 2882.
Chen, Y.-P., Zhang, P., Guo, J.-S., Fang, F., Gao, X., Li, C., 2013. Chemosphere 92, 633–638.
Chio, L., Yang, D., Landry, M., 2017. In: Tiller, T. (Ed.), Synthetic Antibodies: Methods and Protocols. Springer New York, New York, NY:pp. 363–380 http://dx.doi.org/10.1007/978-1-4939-6857-2_23.
Consiglio, R., Randall, N.X., Bellaton, B., von Stebut, J., 1998. Thin Solid Films 332, 151–156.
Cosgrove, T., Heath, T.G., Ryan, K., Crowley, T.L., 1987. Macromolecules 20, 2879–2882.
Das, D., Plazas-Tuttle, J., Sabaraya, I.V., Jain, S.S., Sabo-Attwood, T., Saleh, N.B., 2016. Environ. Sci. Nano. 4, 60–68.
De Gennes, P., 1987. Adv. Colloid Interf. Sci. 27, 189–209.
Decho, A.W., 1990. Oceanogr. Mar. Biol. Annu. Rev. 28, 73–153.
Diegoli, S., Manciulea, A.L., Begum, S., Jones, I.P., Lead, J.R., Preece, J.A., 2008. Sci. Total Environ. 402, 51–61.
Eder, D., Windle, A.H., 2008. Adv. Mater. 20, 1787–1793.
Farkas, J., Peter, H., Christian, P., Gallego Urrea, J.A., Hassellöv, M., Tuoriniemi, J., Gustafsson, S., Olsson, E., Hylland, K., Thomas, K.V., 2011. Environ. Int. 37, 1057–1062.
Flemming, H.-C., Wingender, J., 2010. Nat. Rev. Microbiol. 8, 623–633.
Geranio, L., Heuberger, M., Nowack, B., 2009. Environ. Sci. Technol. 43, 8113–8118.
Giraldo, J.P., Landry, M.P., Faltermeier, S.M., McNicholas, T.P., Iverson, N.M., Boghossian, A.A., Reuel, N.F., Hilmer, A.J., Sen, F., Brew, J.A., Strano, M.S., 2014. Nat. Mater. 13, 400–408.
Giraldo, J.P., Landry, M.P., Kwak, S.-Y., Jain, R.M., Wong, M.H., Iverson, N.M., Ben-Naim, M., Strano, M.S., 2015. Small 11, 3973–3984.
Goldenberg, N.M., Steinberg, B.E., 2010. Cancer Res. 70, 1277–1280.
Harvey, J.D., Jena, P.V., Baker, H.A., Zerze, G.H., Williams, R.M., Galassi, T.V., Roxbury, D., Mittal, J., Heller, D., 2017. Nature Biomedical Engineering 1.
Hauck, T.S., Ghazani, A.A., Chan, W.C.W., 2008. Small 4, 153–159.
Hellstrand, E., Lynch, I., Andersson, A., Drakenberg, T., Dahlbäck, B., Dawson, K.A., Linse, S., Cedervall, T., 2009. FEBS J. 276, 3372–3381.
Hotze, E.M., Phenrat, T., Lowry, G.V., 2010. J. Environ. Qual. 39, 1909–1924.
Hsu, L.-Y., Chein, H.-M., 2007. In: Maynard, A., Pui, D.H. (Eds.), Nanotechnology and Occupational Health. Springer Netherlands:pp. 157–163 http://dx.doi.org/10.1007/978-1-4020-5859-2_15 ch. 15.
Hua, Z., Zhang, J., Bai, X., Ye, Z., Tang, Z., Liang, L., Liu, Y., 2016. Sci. Total Environ. 539, 196–205.
Inomoto, N., Osaka, N., Suzuki, T., Hasegawa, U., Ozawa, Y., Endo, H., Akiyoshi, K., Shibayama, M., 2009. Polymer 50, 541–546.
Jain, A., Liu, R., Ramani, B., Arauz, E., Ishitsuka, Y., Ragunathan, K., Park, J., Chen, J., Xiang, Y.K., Ha, T., 2011. Nature 473, 484–488.
Jain, R.M., Ben-Naim, M., Landry, M.P., Strano, M.S., 2015. J. Phys. Chem. C 119, 22737–22745.
Jose, S., 2009. Agroforestry Systems. 76 pp. 1–10.
Jung, K.-h., Hong, J.S., Vittal, R., Kim, K.-J., 2002. Chem. Lett. 864–865.
Kaegi, R., Ulrich, A., Sinnet, B., Vonbank, R., Wichser, A., Zuleeg, S., Simmler, H., Brunner, S., Vonmont, H., Burkhardt, M., Boller, M., 2008. Environ. Pollut. 156, 233–239.
Kaegi, R., Sinnet, B., Zuleeg, S., Hagendorfer, H., Mueller, E., Vonbank, R., Boller, M., Burkhardt, M., 2010. Environ. Pollut. 158, 2900–2905.
Kaegi, R., Voegelin, A., Sinnet, B., Zuleeg, S., Hagendorfer, H., Burkhardt, M., Siegrist, H., 2011. Environ. Sci. Technol. 45, 3902–3908.
Kang, S., Mauter, M.S., Elimelech, M., 2009. Environ. Sci. Technol. 43, 2648–2653.
Karajanagi, S.S., Vertegel, A.A., Kane, R.S., Dordick, J.S., 2004. Langmuir 20, 11594–11599.
Keller, A.A., Wang, H., Zhou, D., Lenihan, H.S., Cherr, G., Cardinale, B.J., Miller, R., Ji, Z., 2010. Environ. Sci. Technol. 44, 1962–1967.
Khan, I.A., Afrooz, A.R.M.N., Flora, J.R.V., Schierz, P.A., Ferguson, P.L., Sabo-Attwood, T., Saleh, N.B., 2013. Environ. Sci. Technol. 47, 1844–1852.
Khan, I.A., Flora, J.R.V., Afrooz, A.R.M.N., Aich, N., Schierz, P.A., Ferguson, P.L., Sabo-Attwood, T., Saleh, N.B., 2015a. Environ. Chem. 12, 652–661.
Khan, I.A., Flora, J.R., Afrooz, A.N., Aich, N., Schierz, P.A., Ferguson, P.L., Sabo-Attwood, T., Saleh, N.B., 2015b. Environ. Chem. 12, 652–661.
Kim, D.K., Mikhaylova, M., Zhang, Y., Muhammed, M., 2003. Chem. Mater. 15, 1617–1627.
Kiser, M.A., Westerhoff, P., Benn, T., Wang, Y., Pérez-Rivera, J., Hristovski, K., 2009. Environ. Sci. Technol. 43, 6757–6763.
Köhler, A.R., Som, C., Helland, A., Gottschalk, F., 2008. J. Clean. Prod. 16, 927–937.
Kruss, S., Landry, M.P., Vander Ende, E., Lima, B.M.A., Reuel, N.F., Zhang, J., Nelson, J., Mu, B., Hilmer, A., Strano, M., 2014. J. Am. Chem. Soc. 136, 713–724.
Kulikowska, D., Klimiuk, E., 2008. Bioresour. Technol. 99, 5981–5985.
Kumar, S.K., Jouault, N., Benicewicz, B., Neely, T., 2013. Macromolecules 46, 3199–3214.
Landry, M., Kruss, S., Nelson, J., Bisker, G., Iverson, N., Reuel, N., Strano, M., 2014. Sensors 14, 16196.
Landry, M.P., Vuković, L., Kruss, S., Bisker, G., Landry, A.M., Islam, S., Jain, R., Schulten, K., Strano, M.S., 2015. J. Phys. Chem. C 119, 10048–10058.
Landry, M.P., Ando, H., Chen, A.Y., Cao, J., Kottadiel, V.I., Chio, L., Yang, D., Dong, J., Lu, T.K., Strano, M.S., 2017. Nat. Nanotechnol. (advance online publication).
Lau, B.L., Hockaday, W.C., Ikuma, K., Furman, O., Decho, A.W., 2013. Colloids Surf. A Physicochem. Eng. Asp. 435, 22–27.
Lin, D., Tian, X., Wu, F., Xing, B., 2010. J. Environ. Qual. 39, 1896–1908.
Liu, Z., Wang, J., Xie, D., Chen, G., 2008. Small 4, 462–466.
Llobet, E., Espinosa, E., Sotter, E., Ionescu, R., Vilanova, X., Torres, J., Felten, A., Pireaux, J.-J., Ke, X., Van Tendeloo, G., 2008. Nanotechnology 19, 375501.
Louie, S.M., Tilton, R.D., Lowry, G.V., 2016a. Environ. Sci. Nano 3, 283–310.
Louie, S.M., Gorham, J.M., McGivney, E.A., Liu, J., Gregory, K.B., Hackley, V.A., 2016b. Environ. Sci. Nano 3, 1090–1102.
Lowry, G.V., Gregory, K.B., Apte, S.C., Lead, J.R., 2012. Environ. Sci. Technol. 46, 6893–6899.
Lu, D., Xiao, C., Xu, S., 2009. Express Polym Lett 3, 366–375.
Lundqvist, M., Sethson, I., Jonsson, B.-H., 2004. Langmuir 20, 10639–10647.
Mao, J., Hu, W., Schmidt-Rohr, K., Davies, G., Ghabbour, E., Xing, B., 2000. Soil Sci. Soc. Am. J. 64, 873–884.
Mudunkotuwa, I.A., Grassian, V.H., 2015. Environ. Sci. Nano 2, 429–439.
Mulder, J., Cresser, M., Moldan, B., Cerny, J., 1994. Biogeochemistry of Small Catchments, a Tool for Environmental Research. pp. 107–131.
Murphy, E.M., Zachara, J.M., 1995. Geoderma 67, 103–124.
Murphy, E.M., Zachara, J.M., Smith, S.C., 1990. Environ. Sci. Technol. 24, 1507–1516.
Nel, A.E., Mädler, L., Velegol, D., Xia, T., Hoek, E.M.V., Somasundaran, P., Klaessig, F., Castranova, V., Thompson, M., 2009. Nat. Mater. 8, 543–557.
Niederer, C., Schwarzenbach, R.P., Goss, K.-U., 2007. Environ. Sci. Technol. 41, 6711–6717.
O'Sullivan, A.C., 1997. Cellulose 4, 173–207.
Parfitt, R., Fraser, A., Farmer, V., 1977. J. Soil Sci. 28, 289–296.
Pettersson, C., Ephraim, J., Allard, B., 1994. Org. Geochem. 21, 443–451.
Phenrat, T., Saleh, N., Sirk, K., Kim, H.-J., Tilton, R.D., Lowry, G.V., 2008. J. Nanopart. Res. 10, 795–814.
Pigman, W., 2012. The Carbohydrates: Chemistry and Biochemistry. Elsevier.
Plazas-Tuttle, J., Rowles, L., Chen, H., Bisesi, J., Sabo-Attwood, T., Saleh, N., 2015. Nano 5, 1102.
Rao, C.N.R., Müller, A., Cheetham, A.K., 2006. The Chemistry of Nanomaterials: Synthesis, Properties and Applications. John Wiley & Sons.
Rigdon, W.A., Huang, X., 2014. J. Power Sources 272, 845–859.
Roy, R., Hohng, S., Ha, T., 2008. Nat. Methods 5, 507–516.

Saleh, N.B., Pfefferle, L.D., Elimelech, M., 2008. Environ. Sci. Technol. 42, 7963–7969.
Saleh, N.B., Afrooz, A., Bisesi, J.H., Aich, N., Plazas-Tuttle, J., Sabo-Attwood, T., 2014. Nano 4, 372–407.
Saleh, N.B., Aich, N., Plazas-Tuttle, J., Lead, J.R., Lowry, G.V., 2015. Environ. Sci. Nano 2, 11–18.
Sapsford, K.E., Tyner, K.M., Dair, B.J., Deschamps, J.R., Medintz, I.L., 2011. Anal. Chem. 83, 4453–4488.
Sapsford, K.E., Algar, W.R., Berti, L., Gemmill, K.B., Casey, B.J., Oh, E., Stewart, M.H., Medintz, I.L., 2013. Chem. Rev. 113, 1904–2074.
Schlautman, M.A., Morgan, J.J., 1994. Geochim. Cosmochim. Acta 58, 4293–4303.
Schnitzer, M., 1982. Methods of Soil Analysis. Part 2. Chemical and Microbiological Properties. pp. 581–594.
Shvedova, A.A., Kagan, V.E., Fadeel, B., 2010. Annu. Rev. Pharmacol. Toxicol. 50, 63–88.
Smith, M.C., Crist, R.M., Clogston, J.D., McNeil, S.E., 2015. Anal. Bioanal. Chem. 407, 3705–3716.
Somasundaran, P., Krishnakumar, S., 1997. Colloids Surf. A Physicochem. Eng. Asp. 123, 491–513.
Tanford, C., 1980. The Hydrophobic Effect: Formation of Micelles and Biological Membranes. second ed. J. Wiley.
Tanner, C.C., Sukias, J.P., Upsdell, M.P., 1998. Water Res. 32, 3046–3054.
Thurman, E.M., Malcolm, R.L., 1981. Environ. Sci. Technol. 15, 463–466.
Treuel, L., Nienhaus, G.U., 2012. Biophys. Rev. 4, 137–147.
Trivedi, M.V., Laurence, J.S., Siahaan, T.J., 2009. Curr. Protein Pept. Sci. 10, 614–625.
Tsai, D.-H., Davila-Morris, M., DelRio, F.W., Guha, S., Zachariah, M.R., Hackley, V.A., 2011. Langmuir 27, 9302–9313.
Vannote, R.L., Minshall, G.W., Cummins, K.W., Sedell, J.R., Cushing, C.E., 1980. Can. J. Fish. Aquat. Sci. 37, 130–137.
Vargas, A., Shnitko, I., Teleki, A., Weyeneth, S., Pratsinis, S.E., Baiker, A., 2011. Appl. Surf. Sci. 257, 2861–2869.
Wang, X., Liu, L.-H., Ramström, O., Yan, M., 2009. Exp. Biol. Med. (Maywood) 234, 1128–1139.
Wang, X., Chen, X., Liu, S., Ge, X., 2010. J. Environ. Sci. 22, 1960–1965.
Wingender, J., Neu, T.R., Flemming, H.-C., 1999. Microbial Extracellular Polymeric Substances. Springer, pp. 1–19.
Wong, M.H., Misra, R.P., Giraldo, J.P., Kwak, S.-Y., Son, Y., Landry, M.P., Swan, J.W., Blankschtein, D., Strano, M.S., 2016. Nano Lett. 16, 1161–1172.
Wotton, R.S., 2004. Sci. Mar. 68, 13–21.
Yang, P., Meng, X.F., Zhang, Z.Y., Jing, B.X., Yuan, J., Yang, W.T., 2005. Anal. Chem. 77, 1068–1074.
Yang, R., Jin, J., Chen, Y., Shao, N., Kang, H., Xiao, Z., Tang, Z., Wu, Y., Zhu, Z., Tan, W., 2008. J. Am. Chem. Soc. 130, 8351–8358.
Yang, K., Lin, D., Xing, B., 2009. Langmuir 25, 3571–3576.
Yeganeh, B., Kull, C.M., Hull, M.S., Marr, L.C., 2008. Environ. Sci. Technol. 42, 4600–4606.
You, C.-C., De, M., Han, G., Rotello, V.M., 2005. J. Am. Chem. Soc. 127, 12873–12881.
Zeng, H., Gao, C., Wang, Y., Watts, P.C., Kong, H., Cui, X., Yan, D., 2006. Polymer 47, 113–122.
Zhang, Y., Chen, Y., Westerhoff, P., Crittenden, J., 2009. Water Res. 43, 4249–4257.
Zhang, J., Landry, M.P., Barone, P.W., Kim, J.-H., Lin, S., Ulissi, Z.W., Lin, D., Mu, B., Boghossian, A.A., Hilmer, A.J., Rwei, A., Hinckley, A.C., Kruss, S., Shandell, M.A., Nair, N., Blake, S., Sen, F., Sen, S., Croy, R.G., Li, D., Yum, K., Ahn, J.-H., Jin, H., Heller, D.A., Essigmann, J.M., Blankschtein, D., Strano, M.S., 2013. Nat. Nanotechnol. 8, 959–968.
Zhou, D., Keller, A.A., 2010. Water Res. 44, 2948–2956.
Zhu, Y., Elim, H.I., Foo, Y.L., Yu, T., Liu, Y., Ji, W., Lee, J.Y., Shen, Z., Wee, A.T.-S., Thong, J.T.-L., 2006. Adv. Mater. 18, 587–592.